Pergamon

0360-3016(94)E0194-O

rthermia Original Contribution

THE USE OF GENERALIZED CELL-SURVIVAL DATA IN A PHYSIOLOGICALLY BASED OBJECTIVE FUNCTION FOR HYPERTHERMIA TREATMENT PLANNING: A SENSITIVITY STUDY WITH A SIMPLE TISSUE MODEL IMPLANTED WITH AN ARRAY OF FERROMAGNETIC THERMOSEEDS

Dean T. Tompkins, Ph.D.,*[†] Ray Vanderby, Ph.D.,* Sanford A. Klein, Ph.D.,*
William A. Beckman, Ph.D.,* Richard A. Steeves, M.D., Ph.D.[†] and
Bhudatt R. Paliwal, Ph.D.[†]

Departments of *Mechanical Engineering and [†]Human Oncology, University of Wisconsin–Madison, Madison, WI

Purpose: A physiologically based objective function for identifying a combination of ferromagnetic seed temperatures and locations that maximizes the fraction of tumor cells killed in pretreatment planning of local hyperthermia.
Methods and Materials: An objective-function is developed and coupled to finite element software that solves the bioheat transfer equation. The sensitivity of the objective function is studied in the optimization of a ferromagnetic hyperthermia treatment. The objective function has several salient features including (a) a physiological basis that considers increasing the fraction of cells killed with increasing temperatures above a minimum therapeutic temperature ($T_{min,thera}$), (b) a term to penalize for heating of normal tissues above $T_{min,thera}$, and (c) a scalar weighting factor (γ) that has treatment implications. Reasonable estimates for γ are provided and their influence on the objective function is demonstrated. The cell-kill algorithm formulated in the objective function is based empirically upon the behavior of published hyperthermic cell-survival data. The objective function is shown to be independent of normal tissue size and shape when subjected to a known outer-surface, thermal boundary condition. Therefore, fractions of cells killed in tumors of different shapes and sizes can be compared to determine the relative performance of thermoseed arrays to heat different tumors.
Results: In simulations with an idealized tissue model perfused by blood at various rates, maxima of the objective function are unique and identify seed spacings and Curie-point temperatures that maximize the fraction of tumor cells killed. In ferromagnetic hyperthermia treatment planning, seed spacing can be based on maximizing the minimum tumor temperature and minimizing the maximum normal tissue temperature. It is shown that this treatment plan is less effective than a plan based on seed spacings that maximize the objective function.
Conclusions: It is shown that under the assumptions of the model and based on a desired therapeutic goal, the objective function identifies a combination of thermoseed temperatures and locations that maximizes the fraction of tumor cells killed.

Ferromagnetic hyperthermia, Treatment planning, Finite element method, Thermal modeling, Objective function, Cell survival.

INTRODUCTION

The therapeutic goal of a hyperthermia treatment is to raise and maintain the temperature in the tumor, while simultaneously minimizing the temperature increase in surrounding normal tissues. Studies have been performed that optimize temperature distributions in tumor and surrounding normal tissue models by selecting a best set of treatment variables for delivering hyperthermia with various clinical modalities. An *in vivo* study investigated how seed orientation within an electromagnetic coil, in-

terseed spacing, generator power level, and catheters affected temperature distributions achieved with interstitial ferromagnetic hyperthermia (33). A set of simulation input variables has been determined to optimize a heat treatment for multiple electromagnetic applicators (8). A numerical method has been developed to determine power deposition patterns for localized hyperthermia to maintain a uniform temperature throughout a tumor (23). An optimization routine has been used in a two-dimensional theoretical investigation to select the amplitudes and phases of a noninvasive microwave hyperthermia system

for deep-seated tumors (31). Optimal amplitudes and phases have been selected for 915 MHz peripheral sources to focus energy so that power outside a focal region was kept below a threshold (3). Amplitudes and phases have been optimized by comparing the theoretically computed results of eight concentric. fixed microwave apertures and a four-applicator array with movable apertures (38). A theoretical study found that optimal power absorption in cylindrical ferromagnetic implants occurred when the applied magnetic field was axially parallel to the axis of the cylinder and when the induction number is 2.5 (14).

It is commonly assumed that tumor response or control correlates best with minimum temperatures within the tumor ($T_{min,t}$), because clonogens surviving in any region of lower temperature may be a site for regrowth of the tumor (15). Research in this area has shown the importance of steady-state temperatures throughout the tumor being equal to or greater than a minimum temperature (2, 11, 12, 16, 25, 35). However, the predictability of tumor response based on the $T_{min,t}$ descriptor remains poor (10, 24). Other research suggests that the T_{90} and T_{50} temperature descriptors are better predictors than the commonly used $T_{min,t}$ descriptor for eventual histopathological outcome (18). Here, the temperatures that 90% and 50% of all measured tumor temperatures are equal to or greater than are designated as the T_{90} and T_{50} temperatures, respectively (18).

One interpretation of an Arrhenius plot for heat inactivation (or death) of mammalian cells in culture supports the theory that maintaining tumor temperatures above a minimum may be the preferred treatment goal (15). A plot with $1/D_o$ on the ordinate and $1/T_{abs}$ on the abscissa has shown that a significant change in slope occurs between 42 and 43°C (9). T_{abs} is the absolute temperature, while D_o is the reciprocal of the slope of the exponential region of the survival curve (i.e., the time at a given temperature that is necessary to reduce the fraction of surviving cells to 37% of their former value) (15). It is believed that the differences in inactivation energy above and below the 42–43°C temperature range may reflect different mechanisms of cell killing (15). If the goals of a hyperthermia treatment are to maximize tumor cell death and minimize normal cell destruction, use of cell-survival data may provide a basis for an alternative method to select a best set of treatment variables.

Often a best set of hyperthermia treatment variables is determined by maximizing (or. conversely. minimizing) an objective function (i.e., a mathematical equation) that is based on some selected temperature goals for the tissue. For example, several temperature-based objective functions have been developed to determine an optimal set of scanning parameters of an ultrasound hyperthermia system (36). Within the limits of the model and the objective function. a set of treatment variables will be identified to deliver the best heat treatment. The goal of this study is the same as in other optimization studies. but the objective function is fundamentally different than other (temperature-based) objective functions. The objective function in the present study uses hyperthermia cell-survival data where increased cell killing is achieved with increasing temperatures above a threshold temperature. Because hyperthermia cell-survival data are currently incomplete, only an approximation of the tumor (and normal tissue) cell survival can be made at best. Therefore, two models of the hyperthermia cell-survival of the tumor are investigated. Simulations are conducted with an idealized tissue model that is subjected to a single heat treatment. Several constant-rate, nonhomogeneous blood perfusion models are investigated. Under the assumptions of the model. the objective function is used to identify optimum seed spacings and temperatures of thermoseeds within a square implant array. The performance of the objective function is assessed by determining whether the fraction of tumor cells killed is larger than that using the $T_{min,t}$ and maximum normal tissue temperature ($T_{max,n}$) descriptors.

METHODS AND MATERIALS

Bioheat equation

The temperature distributions in the tissue models are determined by solving the steady-state form of the bioheat equation (26):

$$k\nabla^2 T - Wc_b(T - T_b) + q_a = 0 \qquad \text{(Eq. 1)}$$

In Eq. 1, k is the thermal conductivity (W/m/°C); W is the blood perfusion (kg/s/m³); c_b is the specific heat of blood (3900 J/kg/°C); T is tissue temperature (°C); T_b is the blood temperature (°C); q_a is the absorbed energy rate per unit volume of thermoseed (W/m³); and ∇^2 is the Laplacian operator. A discussion on the formulation and limitations of the bioheat transfer equation can be found elsewhere (28).

Often a numerical technique. rather than an analytical approach, can be used to solve for T in Eq. 1. One numerical technique is the finite element method. With this method, a model of the tissue system is divided into several (often hundreds or thousands) smaller regions called finite elements. In the present study, triangular-shaped finite elements, over which the temperature distribution is assumed to be linear, are used as a basis in the finite element equations (21, 32). The temperature distributions are determined using general-purpose. finite-element software (17).

Generalized formulation of objective function

Cell survival curves form the basis of the objective function. The surviving fraction. S (dimensionless). of cells to a single heat treatment is given by (15):

$$S = \frac{\text{colonies counted}}{\text{cells seeded}(PE/100)} \qquad \text{(Eq. 2)}$$

In Eq. 2, *PE* is the plating efficiency, colonies counted are the number of original cells that survive the heat treatment, and cells seeded are the number of cells at the beginning of the heat treatment. Several experiments were conducted so that estimates of survival are obtained for a range of temperatures between 41°C and 47°C and heating times from 30 min to several hours.

It is assumed that cell survival is solely a function of temperature for a preselected exposure time. Thus, cell survival is independent of the cell pH, available oxygen and nutrient levels, and cell cycle. A definition of cell survival relevant to hyperthermia is assumed. In other words, it is assumed that no cells suffer reproductive death until the temperature rises above a certain threshold or minimum therapeutic temperature which we call $T_{min,thera}$. Above $T_{min,thera}$, an increasing fraction of cells suffers reproductive death with increasing temperature. For example, consider the hyperthermia cell-survival data of Chinese hamster (CHO) cells in culture. Below a temperature of about 42°C, a small fraction of cells are killed after hyperthermia exposure times of up to several hours (9). Conversely, with increasing temperatures above approximately 42°C, a dramatically increasing fraction of cells are killed from hyperthermia exposure (9).

The model for simulating cell survival is shown in Fig. 1. This model is not intended to represent the exact cell survival of any particular established cell line to a single heat treatment, but rather hyperthermia cell survival in general. Note that the model does not include an initial shoulder which typically characterizes hyperthermia (and

x-ray) cell-survival data (15). The absence of a shoulder in the cell-survival model is for model simplicity. Although it is known that different cells have different sensitivities to heat, there is no consistent difference in the heat sensitivity between normal and malignant cells (15). One model that we chose for survival of tumor cells is, therefore, equal to the survival of normal cells (Fig. 1, tumor cell model B). In spite of this general observation (i.e., no consistent difference in the heat sensitivity between normal and malignant cells), Robins *et al.* (27) have reported that AKR leukemia cells are more sensitive than normal cells to hyperthermia killing at 41.8°C and 42.5°C. Thus, the present study also investigates the effect of a difference in the sensitivity between normal and malignant cells to heat, with malignant cells being more sensitive (Fig. 1, tumor cell model A).

The cell-survival data are approximated by curves of logarithmic survival, S_{type}, vs. linear temperature (Fig. 1). The fractional cell-survival data are approximated by:

$$S_{type} = 1 \quad \text{when} \quad T \le T_{min,thera} \quad \text{(Eq. 3a)}$$

and

$$S_{type} = 10^{b(T-T_{min,thera})} \quad \text{when} \quad T > T_{min,thera} \quad \text{(Eq. 3b)}$$

In Eq. 3, *type* designates either tumor (*t*) or normal (*n*) cells and *b* is the logarithmic slope of the cell–survival curve. In the simulations in the present study, *b* has a value of −1 for normal tissues and a value of −1 or −2 for tumor tissues (Fig. 1). It can be shown that the curve
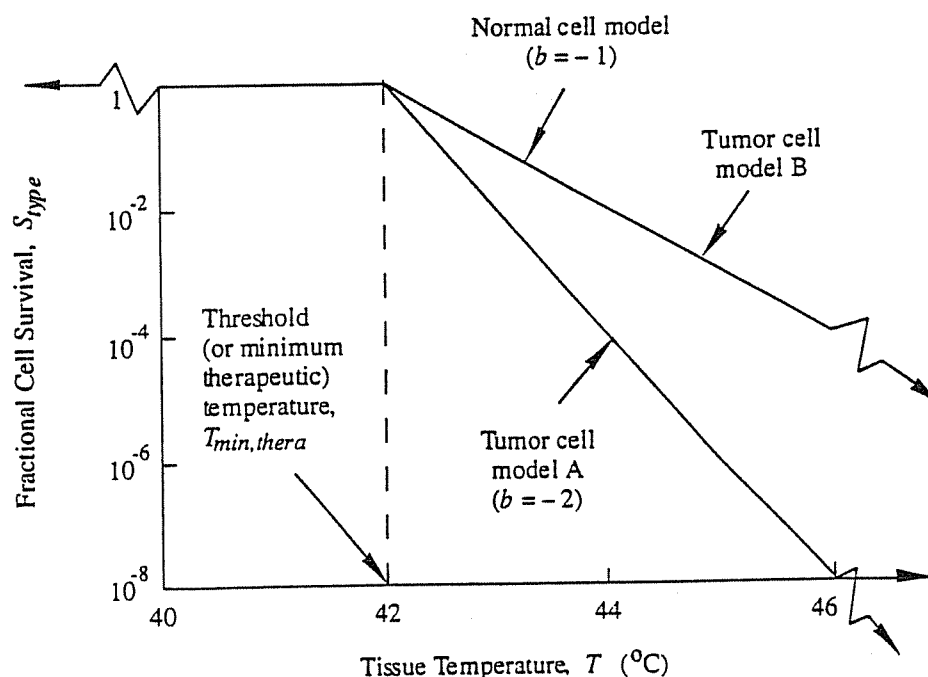

Fig. 1. Models of the fractional cell survival (S_{type}) as a function of tissue temperature (*T*) for tumor and normal cells. It is assumed that the hyperthermia treatment time for this data is 60 min. Two models (A and B) simulating the survival of tumor cells are shown. $T_{min,thera}$ is shown here to be 42°C. The coefficient *b* is the slope of the (logarithmic) cell–survival curves (Eqs. 3–5).

with a slope of -1 is an approximation of survival data of normal CHO cells (9) and human myeloid leukemia cells (K562 line) (20) for an exposure time of approximately 60 min. For other cell-survival models, however, b can have value other than -1 or -2. From analysis of several hyperthermia cell-survival studies. b generally lies between -0.5 and -2.5 for a single heat treatment lasting approximately 60 min (4, 9, 19, 20, 22, 29).

If all cells within a small, *local* volume of tissue were at the same temperature. then Eq. 3 could be used to estimate the fraction of cells surviving the heat treatment. However, because of the spatial dependence of temperature in tissue, a volumetric fraction of surviving cells is estimated by integrating with respect to the volume of cells considered. The *volumetric*, fractional cell survival is designated $S_{V.type}$ and is given by

$$S_{V.type} = 1 \quad when \quad T \le T_{min.thera} \quad (Eq.\ 4a)$$

and

$$S_{V.type} = \frac{\int_{V} 10^{b(T - T_{min.thera})} dV}{\int_{V} dV} \quad when \quad T > T_{min.thera}$$

$$(Eq.\ 4b)$$

In the present study, the finite element method is used to determine the temperature distribution in numerical thermal models of tissue. Thus, Eq. 4 is computed using $S_{V.type}$ within each finite element e comprising the entire tissue model. Therefore, the volumetric fraction of cells surviving a heat treatment in finite element e, $S_{1^{(e)},type}$, is determined by integrating the surviving fraction with respect to the volume of the element, $V^{(e)}$, and then dividing by $V^{(e)}$. The expression for $S_{1^{(e)},type}$ is given by

$$S_{1^{(e)},type} = 1 \quad when \quad T^{(e)} \le T_{min.thera} \quad (Eq.\ 5a)$$

and

$$S_{V^{(e)},type}$$
$$= \frac{1}{V^{(e)}} \int_{1^{(e)}} 10^{b(T^{(e)} - T_{min.thera})} dV \quad when \quad T^{(e)} > T_{min.thera}$$

$$(Eq.\ 5b)$$

In Eq. 5, $T^{(e)}$ is the spatially dependent temperature within finite element e. Thus, within each finite element, the surviving fraction of cells which is below $T_{min.thera}$ is evaluated with Eq. 5a. while the fraction that is above $T_{min.thera}$ is evaluated with Eq. 5b.

The volumes occupied by models of each cell type (either tumor or normal) consist of several finite elements.

Thus, the fraction of cells killed of each cell type during a single heat treatment is given by:

$$\psi_{type} = \frac{\overset{\substack{Total\ Number\ of \\ Finite\ Elements \\ of\ type}}{\sum_{e=1}} (1 - S_{1^{(e)},type}) V^{(e)}}{V_t} \quad (Eq.\ 6)$$

In Eq. 6. V_t is the total volume of tumor cells in the tissue model. In words, the formulation of Eq. 6 is as follows. The volumetric surviving fraction of cells in finite element e is subtracted from 1 to give the fraction of cells killed. Then the fraction of cells killed in finite element e is weighted by $V^{(e)}$, and this product is summed for all finite elements of *type*. The numerator is then divided by V_t to determine ψ, the fraction of cells killed in volume V_t.

By dividing by V_t in Eq. 6, comparisons can be made of ψ_t between tumors with different volumes (see Appendix). Further, by dividing by V_t instead of V_{type}, ψ_n will have a larger magnitude with tissue models where $V_n > V_t$. A tissue model where $V_n > V_t$ is a thermal modeling condition that can be encountered frequently. It is discussed later how larger ψ_ns provide greater sensitivity in the objective function than that using smaller ψ_ns. ψ_n is independent of the size and shape of normal tissue considered so long as the temperatures at the vertices (or corners) of the finite elements in normal tissue at a sufficient distance from the heat sources are below $T_{min.thera}$. In other words. $S_{1^{(e)},n} = 1$ for these finite elements and does not contribute to the summation in the numerator of Eq. 6. Because thermal modelers are free to select the location of the outer surface of normal tissue and subject only to known boundary conditions. the formulation of ψ_n in Eq. 6 has the advantage of being independent of the size and shape of normal tissue.

The objective function consists of two terms and is given by:

$$F = \gamma \psi_t - (1 - \gamma) \psi_n \quad (Eq.\ 7)$$

The first term on the right-hand side of the Eq. 7 is the fraction of tumor cells killed multiplied by a scalar weighting factor. γ. It is common practice in the formulation of an objective function to include a weighting factor. Depending on the value of the weighting factor, a particular. predesired condition or outcome is favored over other possible outcomes. In Eq. 7, values for γ are between 0 and 1. Criteria that must be considered to select the magnitude of γ are discussed later. Thus, in Eq. 7 the product $\gamma \psi_t$ is a weighted fraction of the tumor cells killed. The second term on the right-hand side of Eq. 7 is the fraction of normal cells killed that is multiplied by $(1 - \gamma)$. This second term is the penalty portion of the objective function. Because it is desired to maximize the fraction

Table 1. Guide for selecting γ

Hyperthermia pretreatment design considerations	Weighting factor, γ
Therapeutic goal	
1) Minimize normal tissue complications	0.2–0.5
2) Compromise between minimizing normal tissue complications & maximizing tumor cell death	0.6–0.8
3) Maximize tumor cell death	0.9–1
Thermal tolerance of normal cells near tumor periphery	
1) Low	0.2–0.5
2) High	0.9–1

of tumor cells killed. there is a penalty[1] for heating normal tissue cells above $T_{min.thera}$. Therefore, the second term is subtracted from the first. In the limit, when $\gamma = 1$, the objective function (F) has an upper limit that approaches 1. When $\gamma = 0$, the objective function has a negative, lower limit that will approach the ratio of the volume of normal tissue, V_n, to the volume of tumor tissue, V_t.

The value of γ in Eq. 7 is specified by the clinician for each individual patient, depending upon the clinician's experience and judgment of the patient's overall needs and clinical condition. A guide for the selection of γ is shown in Table 1. A treatment plan with $\gamma = 0$ or near 0 would be impractical. When $\gamma = 0$, the optimization process would seek seed spacings and Curie points that would completely minimize heating of normal tissue cells. In itself. completely minimizing normal tissue heating is desired, but in so doing, this would significantly minimize heating of the tumor. If the desired treatment goal is to minimize normal tissue heating and there is a modest concern for maximizing tumor tissue heating. then γ should have a value between 0.2 and 0.5. If the treatment plan is designed to maximize the fraction of tumor cell death and there is modest concern for normal tissue heating, then γ should have a value between 0.6 and 0.8. Last, if the desired treatment goal is to maximize the fraction of tumor cell death without concern for normal tissue heating. then γ should have a value between 0.9 and 1. The magnitudes for γ between 0.2 and 1 as discussed above are assumed values. Although a treatment plan with $\gamma = 1$ will maximize the fraction of tumor cell death. normal tissues will not be spared and may result in significant heating of normal tissue cells near the tumor boundary. Thus. a treatment plan with $\gamma = 1$ should be used with caution. If the thermal tolerance of normal tissue cells on the boundary of the tumor are low (i.e.. a large $-b$ value in Eqs. 3–5 and Fig. 1), then γ should have a value between 0.2 and 0.5. If normal tissue cells on the

boundary can tolerate temperatures above $T_{min.thera}$ (i.e.. a small $-b$ value). then γ should have a value between 0.9 and 1. In summary. choices of the weighting factor are not arbitrary but guidelines for the selection of γ and reasonable estimates are provided in Table 1.

Once a particular value for the weighting factor is selected and models of the blood perfusion in tumor and normal tissues have been assumed. the mathematical goal is to maximize the objective function (F) over a range of values of hyperthermia treatment variables. In the present study, ferromagnetic hyperthermia treatment variables that are investigated include interseed spacing between seeds and the Curie temperatures of each seed in the array.

Accuracy of numerically computed objective function

The accuracy of the algorithm in computing the objective function numerically can be established. Analytical solutions for the fraction of tissue cells killed (ψ_t and ψ_n) and the objective function (F) are compared to numerical solutions in simulations with a simple tissue model perfused with blood at various rates.

Analytical model. The model is of a single seed centered in an infinitely long. cylindrical tissue system. The analysis is developed for the cross-sectional area. A, of the tissue for simplicity at this stage (Fig. 2). Heat flow in the tissue model is assumed to be radially dependent. The tissue model consists of a seed of radius a, surrounded by shell-shaped tumor tissue with radial boundaries a and r_t. Surrounding the tumor is shell-shaped normal tissue with radial boundaries r_t and r_n. The solution for the temperature θ ($= T - T_b$) in the tissue model as a function of radial distance has been derived previously (34) and is given by:

$$\theta(r) = \frac{P'a}{2A_{c.s}mk} \frac{[I_0(mr_n)K_0(mr) - K_0(mr_n)I_0(mr)]}{[I_1(ma)K_0(mr_n) + I_0(mr_n)K_1(ma)]}$$

(Eq. 8)

In Eq. 8. P' is the absorbed power of the seed (W/m); $A_{c.s}$ is the cross-sectional area of the seed (m²); m is a parameter ($= \sqrt{Wc_b/k}$) (m⁻¹); I_0 and K_0 are modified Bessel functions of the first and second kind of order 0. respectively (1); and I_1 and K_1 are modified Bessel functions of the first and second kind of order 1, respectively (1). Substituting Eq. 8 into Eq. 4b gives:

$$S_{A.type} = \frac{1}{A} \int_A 10^{b[(T_b+\theta)-T_{min.thera}]} dA \qquad (Eq.~9)$$

---

[1] Subjecting the tumor to very high temperatures will most likely kill all tumor cells but will also cause severe damage to surrounding normal tissue cells. Thus. a penalty term in the objective function is necessary.
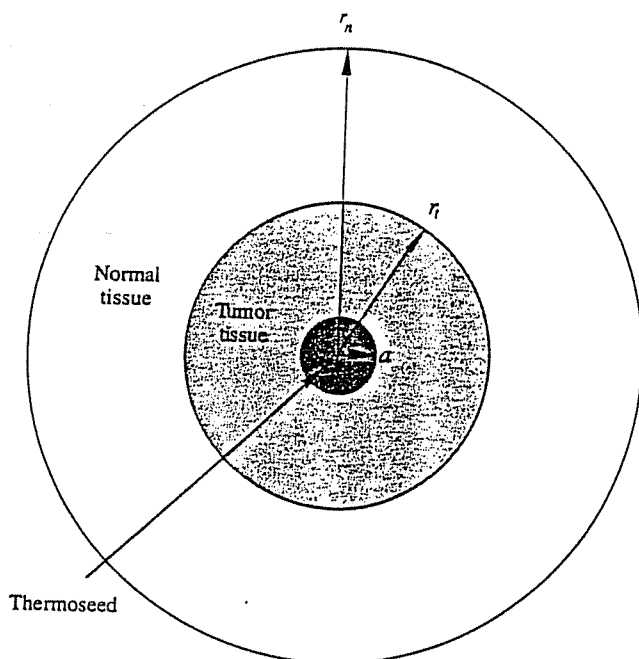
Fig. 2. Single seed centered in a cross-section of a cylindrical tissue model. The seed, tumor, and normal tissue have outer radii of a, r_t, and r_n, respectively. Radial lengths shown are not to scale. Thermal boundary condition at r_n is $T(r_n) = T_b$.

With a change in the variable of integration, Eq. 9 becomes:

$$S_{A,type} = \frac{2\pi}{A} \int_{r_k}^{r_l} 10^{b[(T_b+\theta)-T_{min,thermal}]} r dr$$

$$= \frac{2}{(r_l^2 - r_k^2)} \int_{r_k}^{r_l} 10^{b[(T_b+\theta)-T_{min,thermal}]} r dr \qquad (Eq.\ 10)$$

Evaluation of Eq. 10 for tumor and normal tissue cells and values of r_l and r_k are as follows. For the tumor, $r_k = a$ and r_l is the radius of the tumor, r_t, or the radius of the $T_{min,thera}$ isotherm, whichever is smaller. For normal tissue, if r_t is smaller than the radius of the $T_{min,thera}$ isotherm, then $r_k = r_t$ and r_l is the radius of the $T_{min,thera}$ isotherm. Otherwise, r_t is larger than the radius of the $T_{min,thera}$ isotherm and all of the normal tissue cells survived. Thus, in the latter case $S_{A,n} = 1$. With the fraction of cell survival, $S_{A,type}$, determined for normal and tumor tissues, ψ_{type} can be computed with:

$$\psi_{type} = \frac{(1 - S_{A,type})A_{type}}{A_t} \qquad (Eq.\ 11)$$

Equation 11 is used for determining ψ_{type} for tumor and normal tissue cells. Equation 11 can now be used to evaluate Eq. 7 for the objective function F. Because the temperature θ inside the integral in Eq. 10 contains several

Bessel functions (Eq. 8), the integration of Eq. 10 is evaluated with Mathematica (37). The input data and solution of the integration of Eq. 10 as performed by Mathematica is shown elsewhere (32).

Numerical model. In the analytically computed fractional cell survival, $S_{A,type}$, above, an integration (Eq. 10) is performed over a tissue model where the temperature distribution is continuous (Eq. 8). However, the numerical model will require an integration over each finite element in the mesh because the temperature distribution between adjacent elements is piece-wise continuous. It can be shown with some algebra (32) that Eq. 5b is:

$$S_{A^{(e)},type} = \frac{1}{A^{(e)}} \int_{y_2}^{y_1} \int_{x_i}^{x_j} 10^{b[(a_1+a_2x+a_3y)-T_{min,thermal}]} dx\, dy$$

$$+ \frac{1}{A^{(e)}} \int_{y_3}^{y_1} \int_{x_j}^{x_k} 10^{b[(a_1+a_2x+a_3y)-T_{min,thermal}]} dx\, dy \quad (Eq.\ 12)$$

where

$$a_1 = \frac{1}{2A^{(e)}} [(x_jy_k - x_ky_j)T_i^{(e)}$$

$$+ (x_ky_i - x_iy_k)T_j^{(e)} + (x_iy_j - x_jy_i)T_k^{(e)}]$$

$$a_2 = \frac{1}{2A^{(e)}} (-y_{jk}T_i^{(e)} + y_{ik}T_j^{(e)} - y_{ij}T_k^{(e)})$$

$$a_3 = \frac{1}{2A^{(e)}} (x_{jk}T_i^{(e)} - x_{ik}T_j^{(e)} + x_{ij}T_k^{(e)})$$

In Eq. 12, $T_i^{(e)}$, $T_j^{(e)}$, and $T_k^{(e)}$ are the temperatures at vertices i, j, and k of finite element e, and $y_{jk} = y_k - y_j$, etc. The variables x_i, x_j, x_k, y_i, y_j, y_k, y_1, y_2, and y_3 are shown in Fig. 3. The integration of Eq. 12 is performed with Mathematica to obtain a general form of the solution that can be found elsewhere (32). The general solution to Eq. 12 reveals that the surviving fraction of cells ($S_{A^{(e)},type}$) is a function of (a) the temperatures (T_i, T_j, and T_k) in a spatial (finite) element containing several cells of *type*, (b) the slope (b) of the survival curve, and (c) $T_{min,thera}$ (32). Equation 12 is used to evaluate Eqs. 6 and 7 for ψ_{type} and F, respectively.

The numerical model consists of a finite element mesh of the seed, tumor, and normal tissue system (Fig. 2). The seed is simulated with a dodecagonally shaped model in which the seed temperature is assumed uniform over its cross-section (32, 34). A parametric study is performed with uniform blood perfusion rates between 0.1 and 10 kg/s/m^3 in the tumor and normal tissue. The energy absorption rate ($q_a = P'/A_{c,s}$) of the numerical (and analytical) seed models are determined at each perfusion rate so that the seed temperature is 60°C. Here, the seed temperature is constrained so that the calculation of the objective function by the analytical method can be compared
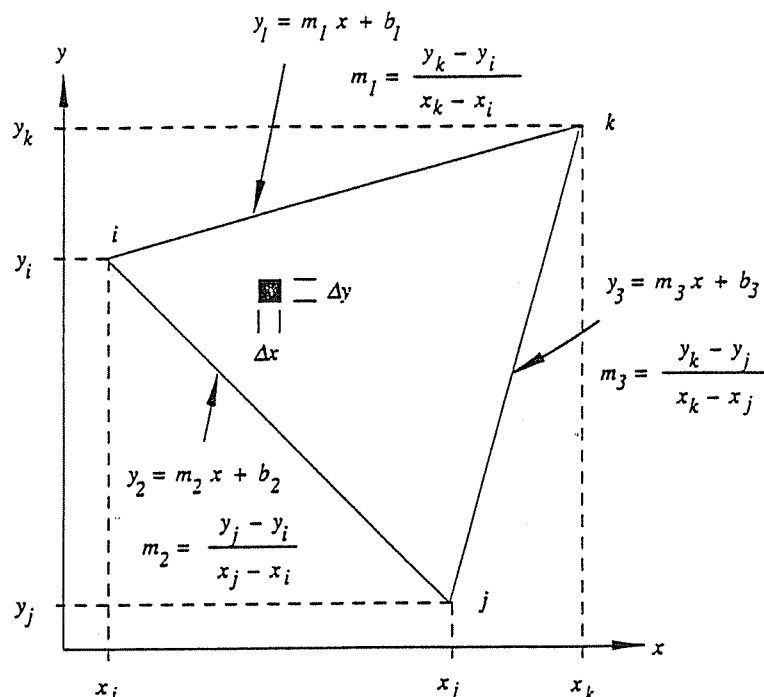
Fig. 3. Example of finite element in which integrations in Eq. 12 are performed. The finite element has vertices i, j, and k. The general (linear) equation fit for the three element lines connecting the vertices are shown. The slopes of the finite element lines are designated by m_1, m_2, and m_3.

with that of the numerical method.[2] A mesh consisting of 603 finite elements is sufficient for accuracy of the numerical tissue model (32). ·

Simulations

Simulations are performed on a square tissue model[3] with a tumor length of $2L_t$ and a normal tissue length of $2L_n$ (Fig. 4). Earlier studies (13) and clinical experience have shown that often, the inner core of the tumor is tough and fibrous and may have blood perfusion that differs vastly from that in the outer periphery of the tumor. Thus, the tumor is modeled as two distinct regions consisting of an inner core and an outer periphery. The tumor model is implanted with a 4 × 4 square array of seeds with Curie points of 53.0, 57.6, and 62.6°C. The 53.0°C-type array consists of 16 seeds with Curie points of 53.0°C. Similarly, the 57.6°C- and 62.6°C-type arrays consist only of seeds with Curie points of 57.6 and 62.6°C, respectively. The preceding three seed configurations are considered uniformly loaded arrays. To study the effect of placing

warmer seeds near the tumor periphery and lower-temperature seeds near the center of the thermoseed array, simulations are performed with a differentially loaded seed array. The differentially loaded seed array consists of a combination of eight 57.6°C-type, four 62.6°C-type, and four 53.0°C-type seeds. The 57.6°C-, 62.6°C-. and 53.0°C-type seeds are located at seed positions 1, 2, and 3, respectively, in Fig. 4. Simulations are conducted with arrays of bare seeds that are spaced uniformly in the x and y directions with an interseed spacing, l, between 9 and 15 mm. All simulations are performed with a finite element mesh of a symmetrical portion (1/8) of the tissue model shown in Fig. 4. The finite element mesh has adiabatic (no heat flow) boundaries at $x = 0$ and $y = x$ and a constant-temperature (T_b) boundary at $y = L_n$. A mesh of 1530 elements is adequate for numerical accuracy (32, 34).

A finite element thermal model (32, 34) of the seeds is used in the simulations. An iterative technique is used to determine the temperature. $T_s(q_a)$, of *each* seed for the

---

[2] It has been shown with the tissue system in Fig. 2. that when the seed model is constrained by power (P'). seed and tissue temperatures determined with the numerical seed model are within 0.1°C of the analytical model (34). In the present paper. if the seed had been constrained by P', then the error in the numerically computed objective function would be confounded with the error in the numerical seed model.

[3] It has been shown that two-dimensional vs. three-dimen-

sional modeling of ferromagnetic hyperthermia in tissue models is adequate so long as the cross-section that is modeled is further than 10 mm from the ends of the thermoseeds (6) and that the thermoseeds are longer than 30 mm and the cross-section is the centrally located plane (5). The cross-sections in Fig. 4 and thermoseed lengths (> 50 mm) used in this study satisfy these requirements.
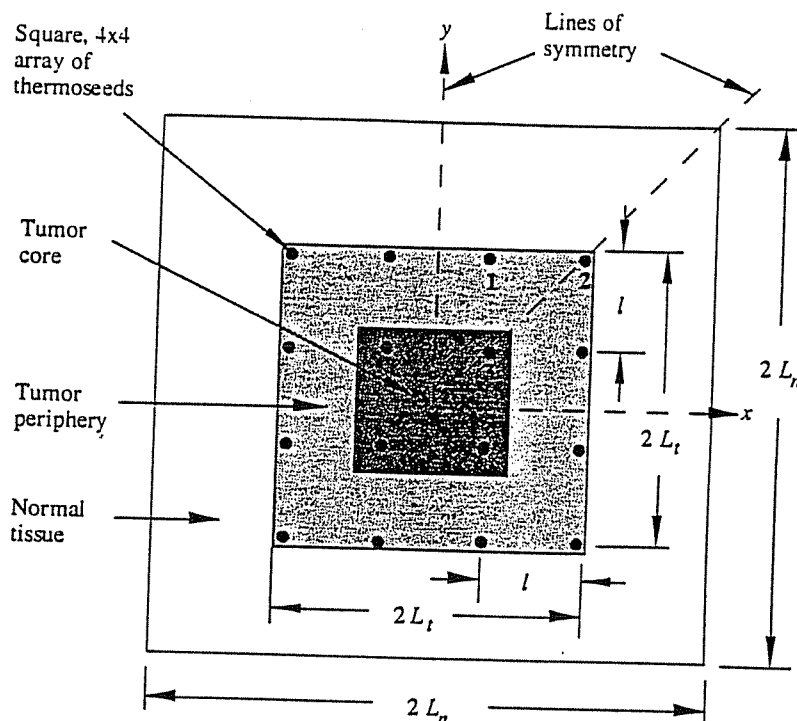
Fig. 4. Two-dimensional cross-section of a square tissue model consisting of a tumor core, tumor periphery, and surrounding normal tissue. The lengths of the tumor core, tumor periphery, and normal tissue are 24 mm, 47 mm ($= 2L_t$), and 180 mm ($= 2L_n$), respectively. Seed locations are represented by black circles and are separated uniformly by a distance l. Thermoseeds 1, 2, and 3 are numbered for reference.

power absorbed (q_a) (32, 34). In the calculation of the absorbed power, $\sigma = 2.57 \times 10^6$ $(\Omega\text{-m})^{-1}$, $H_o = 3.98 \times 10^3$ A/m, $\mu_o = 10 \times 10^{-7}$ tesla-m/A, $f = 90$ kHz, and μ is a function of T_s (32, 34). All tissues are perfused by blood at T_b (37°C). The thermal conductivity of the muscle and tumor tissues is 0.64 W/m/°C. Three constant-rate blood perfusion models are used in the simulations (Table 2). Blood perfusion models 1 and 2 assume there is a uniform rate of perfusion in the tumor. Blood perfusion model 3 is a nonuniform model where the perfusion in the tumor periphery [(p) in Table 2] is 7.5 times greater than that in the tumor core [(c) in Table 2] and 1.5 times greater than that in the normal tissue.

RESULTS

Accuracy of numerically computed objective function

The predicted fraction of cells killed in the tumor (ψ_t) and normal tissue (ψ_n) and the objective function (F) as a function of blood perfusion are shown in Fig. 5. Over 2 decades of blood perfusion, the error in determining ψ_{type} and F with the numerical model is quite small.

Effect of tumor survival model

The fraction of tumor cells killed and the objective function vs. seed spacing for the two models simulating the survival of tumor cells are shown in Fig. 6. Because tumor cell survival model A has a steeper slope ($b = -2$) than model B ($b = -1$), more tumor cells are killed in simulations using model A than model B at the same temperature. In all simulations, therefore, the objective function is larger with tumor cell survival model A. The curves reveal that the objective function is weakly dependent on differences between tumor cell survival models A and B. Thus, results from the remaining simulations are shown for tumor cell survival model B.

Effect of weighting factor

The objective function vs. seed spacing in simulations with all three perfusion models is shown in Fig. 7. The weighting factor has an influence on optimal seed spacing in simulations with low-to-moderate blood perfusion (model 1) but has a negligible influence with moderate-to-high blood perfusions (models 2 and 3). A very small fraction of normal tissue cells is killed (ψ_n) at optimal seed spacings in simulations with high blood perfusion (model 3) (Fig. 7d). Conversely. measurable fractions of normal
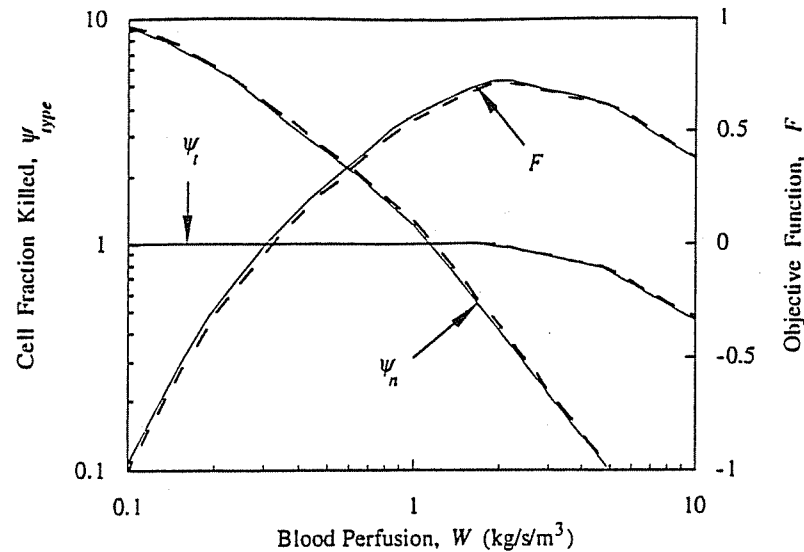
Table 2. Blood perfusion models

Blood perfusion model	Blood perfusion, W (kg/s/m³)	
	Tumor	Normal tissue
1	1.9	4.77
2	4.77	9.54
3	1.9 (c); 14.3 (p)	9.54

Fig. 5. The fraction of cells killed ψ_{type} and the objective function F vs. blood perfusion. The analytical solutions (solid lines) are determined with Eqs. 7, 10, and 11. The solutions predicted by the numerical model (dashed lines) are computed with Eqs. 6, 7, and 12. In the simulations, $a = 0.45$ mm, $r_t = 5$ mm, $r_n = 100$ mm, $k = 0.64$ W/m/°C, $T_s = 60$°C, $\gamma = 0.8$, and there is uniform perfusion in the tumor and normal tissue (Fig. 2).
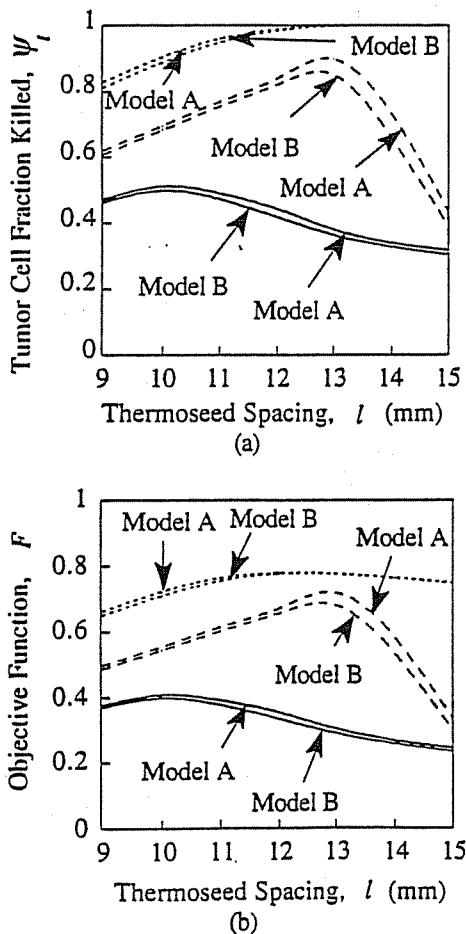

Fig. 6. Effect of tumor survival models A and B on the (a) fraction of tumor cells killed and (b) objective function. Simulations are performed with $\gamma = 0.8$ and with an array of bare seeds with a Curie point of 62.6°C. Curves are shown for blood perfusion models 1 (short dashed lines), 2 (long dashed lines), and 3 (solid line).

tissue cells are killed in low perfusion cases (model 1) (Fig. 7d). Thus, the weighting factor has an influence on optimal seed spacing for configurations of seeds that heat the tumor sufficiently so that a fraction of normal tissue cells near the tumor-normal tissue boundary is killed (i.e., heated above $T_{min.thera}$).
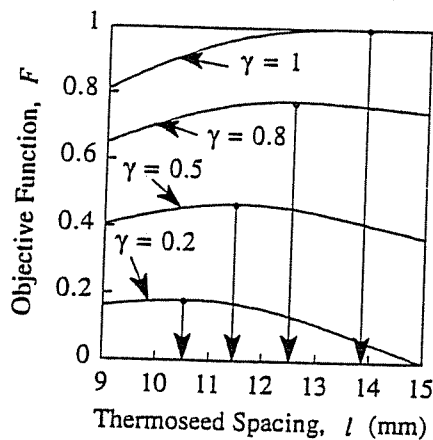
Therapeutic assessment of objective function

Seed designs that maximize the objective function are in Table 3. The objective function is maximized with the array of 62.6°C-type seeds at all γs when tumor blood perfusion is in the moderate-to-high range (models 2 and 3). Although the differentially loaded configuration maximizes F in three simulations, the objective functions from simulations with the 57.6°C-type design are very close to those of the differentially loaded design.
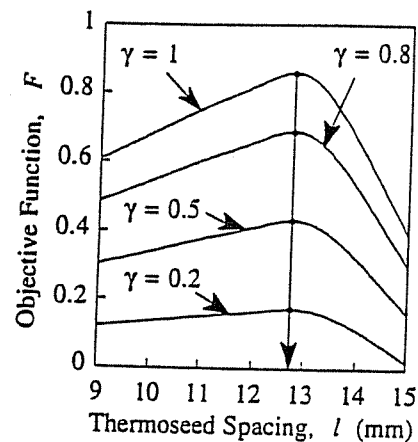
In simulations with the 62.6°C-type design, seed spacings (l_{opt}) that maximize $T_{min.t}$ and attain a $T_{max.n}$ of 45°C are shown in Fig. 8a and b for blood perfusion models 2 and 3, respectively. The tumor cell fractions killed vs. seed spacing for the same design are shown in Figs. 8c and d for blood perfusion models 2 and 3, respectively. Additionally, the seed spacings (l_{opt}) from maximizing the objective function, maximizing $T_{min.t}$ and attaining $T_{max.n}$ = 45°C are shown (Figs. 8c and d). Ψ_t is higher with l_{opt} based on the objective function than with l_{opt} based on temperature descriptors. Indeed, with blood perfusion model 3, ψ_t is about 47% higher (0.5 vs. 0.34) with $l_{opt.F}$ than with l_{opt} based on maximizing $T_{min.t}$ or attaining $T_{max.n}$ = 45°C.
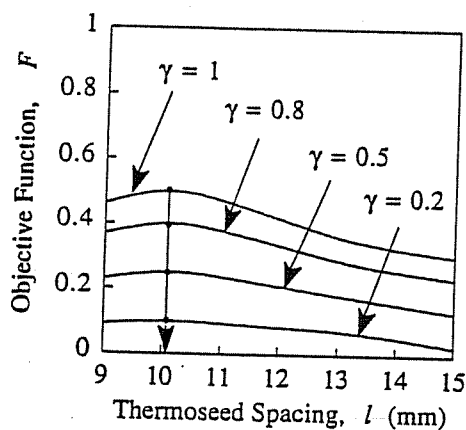
DISCUSSION

The goal of the present study is to formulate and subsequently test a physiologically based objective function.

(a) Blood perfusion model 1

(b) Blood perfusion model 2
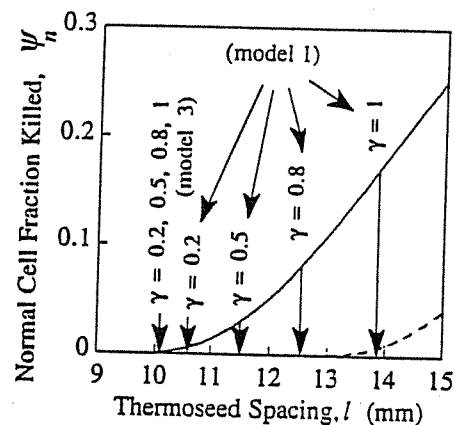

(c) Blood perfusion model 3

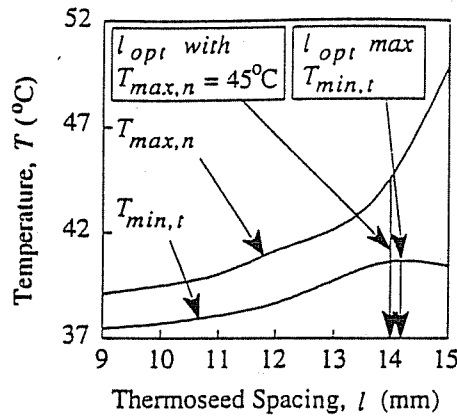(d) ψ_n for blood perfusion models 1 (solid line) and 3 (dashed line)

Fig. 7. Objective function vs. seed spacing for several weighting factors. Simulations are performed with blood perfusion models (a) 1, (b) 2, and (c) 3. The fraction of normal tissue cells killed is shown in part (d) for blood perfusion models 1 (solid line) and 3 (dashed line). Simulations are performed with an array of 62.6°C-type seeds and tumor survival model B. Maxima of the objective function are shown with vertical arrows. All curves of F with $\gamma = 1$ are plots of the tumor cell fraction killed, ψ_t.

The objective function uses hyperthermia cell-survival data where increased cell killing is achieved with increasing temperatures above a threshold temperature. Generalized approximations of hyperthermia cell-survival data are made for the tumor and normal tissue cells. Simulations are conducted with an idealized tissue model that is sub-
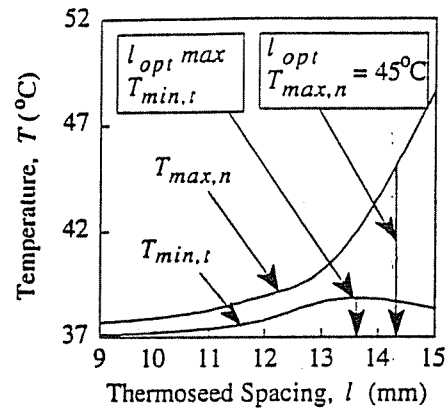
jected to a single heat treatment. Several constant-rate, nonhomogeneous blood perfusion models are investigated. Under the assumptions of the model, the objective function is used to identify optimum seed spacings and temperatures of thermoseeds in ferromagnetic hyperthermia. The performance of the objective function is assessed

Table 3. Seed designs that maximize objective function

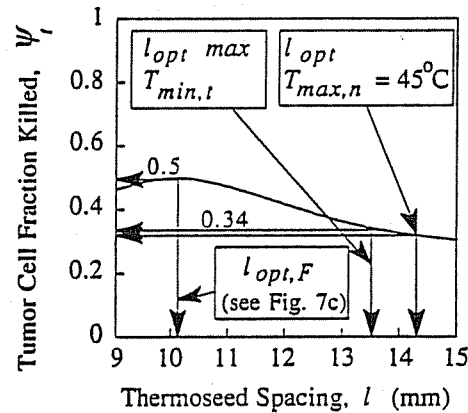| Blood perfusion model	Array Type (seed spacing, l (mm))			
	$\gamma = 0.2$	$\gamma = 0.5$	$\gamma = 0.8$	$\gamma = 1$
1	Diff.-Loaded (12.0)	Diff.-Loaded (12.4)	Diff.-Loaded (13.1)	62.6 (13.8)
2	62.6 (12.7)	62.6 (12.7)	62.6 (12.7)	62.6 (12.7)
3	62.6 (10.1)	62.6 (10.1)	62.6 (10.1)	62.6 (10.1)

(a) Blood perfusion model 2

(b) Blood perfusion model 3

(c) Blood perfusion model 2

(d) Blood perfusion model 3

Fig. 8. Effect of seed spacing on $T_{min,t}$ and $T_{max,n}$ temperatures with blood perfusion models (a) 2 and (b) 3 in simulations with 62.6°C-type seeds. Fraction of tumor cells killed vs. seed spacing for the 62.6°C-type seed design with perfusion models (c) 2 and (d) 3. Seed spacings that maximize the objective function ($l_{opt,F}$), maximize $T_{min,t}$ ($l_{opt,max}$ $T_{min,t}$) and attain $T_{max,n} = 45°C$ (l_{opt}, $T_{max,n} = 45°C$) are labeled.

by determining whether the fraction of tumor cells killed is larger than that using the $T_{min,t}$ and $T_{max,n}$ temperature descriptors. The inclusion of a model in the objective function that exploits the temperature dependence of hyperthermia cell survival is novel. Several other hyperthermia-applied, objective functions are temperature based, but do not directly model the effect of increased cell killing with higher temperatures. Thus, incorporating cell biology in hyperthermia simulation studies may, in fact, be significant and is under investigation by others (7).

The results from simulations with the idealized tissue model are significant. The curves in Fig. 8c and d indicate that, under the assumptions of the tissue model, the objective function identifies seed spacings that maximize the fraction of tumor cells killed. Moreover, the objective function (F) out-performs the method of choosing seed spacings based on $T_{min,t}$ and $T_{max,n}$ temperature descrip-

tors. In other words, a smaller (than the maximum) fraction of tumor cells is killed when seed spacing is based on maximizing $T_{min,t}$ or attaining $T_{max,n} = 45°C$ than when the treatment plan is based on a seed spacing that maximizes F. A possible explanation for this result is that ψ_t (= F when $\gamma = 1$) depends on the (piece-wise) continuous temperature distribution throughout the entire tissue model and incorporates a method to model increased cell killing with increasing temperatures above $T_{min,thera}$. Conversely, $T_{min,t}$ and $T_{max,n}$ are based only on temperatures at discrete locations (i.e., finite-element nodes) in the tissue model.

The above explanation, coupled with the results (Fig. 8c and d) from the present theoretical study, may support the previous clinical observation that the T_{90} and T_{50} temperature descriptors are better predictors of tumor response (i.e., patient survival) than $T_{min,t}$ (18). T_{90} and T_{50} are temperature descriptors determined from a compi-

lation of numerous temperature samples measured throughout the tumor over the entire hyperthermia treatment, including the relatively short transient period at the beginning of the treatment. Therefore, the clinically determined T_{90} and T_{50} descriptors may be related. in part. to the theoretically predicted ψ_t. Thus, there is evidence that $T_{min,t}$, as measured either in the clinic (18) or predicted a priori via modeling (Fig. 8), is less of a predictor of tumor response than maintaining high T_{90} and $T_{50}s$, that are related, in part, to maximizing the theoretically computed ψ_t.

The objective function could be used to identify optimal seed combinations with treatment plans that desire to achieve a compromise between maximizing the fraction of tumor cells killed and minimizing normal tissue heating. Satisfactorily achieving this compromise may be the most frequently encountered treatment consideration. In some cases it may be difficult to determine an optimal treatment plan based on a compromise between maximizing $T_{min,t}$ and minimizing $T_{max,n}$ with only $T_{min,t}$ and $T_{max,n}$ information available through simulations a priori. In these cases, the single-valued, maximum of the objective function with $\gamma = 0.8$ (or close to 0.8) could identify an optimum combination.

The objective function is not formulated to consider patient pain directly. In other words, there is no term in the formulation of F (Eq. 7) that accounts directly for pain. Indirectly, though, the weighting factor could be used to consider patient pain. A value for γ between 0.2 and 0.5 could be used in treatment planning of patients who have a low threshold of pain. Conversely, a value for γ between 0.8 and 1 could be used for patients with a high threshold of pain.

The seed combinations identified by the objective function as desirable are based on discrete values in the Curie point of the seeds. It is possible, though, that the objective function can be maximized with Curie points between 53.0 and 62.6°C or higher. Thus, in addition to the Curie points investigated herein, the objective function could also be maximized by performing a continuous search for the optimal Curie point of each seed. However, the availability of seeds in the clinic with different Curie points is limited; typically between one and three, different Curie temperatures are available.

Optimal seed combinations will depend on assumed models of the blood perfusion. In the present paper where the effect of blood perfusion on the heating of tissue is modeled with a linear sink term (26), the most desirable seed combination with $\gamma = 0.2, 0.5$, and 0.8, depends on the blood perfusion model (Table 3). Because the Pennes equation does not adequately describe the effect of large blood vessels on tissue temperature. the results of the manuscript are limited under the assumption of the model herein. Thus, it is critical that the most accurate model of blood perfusion be used in simulations.

It is well known that there is a complementary cell

killing effect when heat is combined with another modality (e.g.. radiation or chemotherapy). yet only the cytotoxic effect of heat alone has been considered in the present study. The present study is concerned with simply maximizing tumor cell kill from the hyperthermia component of a multimodality therapy regimen. Through the weighting factor (γ), the approach used herein incorporates a method to account for complications from normal tissue heating.

To take advantage of the increased level of tumor kill at a seed spacing that maximizes F vs. that which maximizes $T_{min,t}$, precision in seed placement may have to be near 1 mm (Fig. 8c). It is likely that this degree of precision is not possible in a high percentage of implant procedures. Thus, the results of Figs. 6 and 8 indicate that the tumor response model is not particularly important. but the quality of the implantation procedure is critical.

The two-dimensional aspects of the present study need to be extended to three dimensions. Studies comparing the temperature distributions from two- and three-dimensional models of ferromagnetic seeds have shown that two-dimensional modeling is sufficient only under certain conditions (5. 6). Additionally, because there is some interest in concurrent brachytherapy and ferromagnetic hyperthermia which combines alternately, short (4 mm) radiation and ferromagnetic seeds end-to-end in catheters (30), complete three-dimensional modeling will be necessary.

CONCLUSION

A physiologically based objective function is developed and coupled to a finite element program that solves the bioheat equation. The objective function has several salient features. First, the objective function has a physiological basis and considers increased cell killing with increasing temperatures above a minimum therapeutic level ($T_{min,thera}$). Second. there is a penalty term in the objective function to account for heating of normal tissue cells above $T_{min,thera}$. Third, because normal tissues below $T_{min,thera}$ are eliminated in the determination of the fraction of normal tissue cells killed, the objective function is independent of normal tissue size and shape when subject to a known outer-surface, thermal boundary condition. The fraction of tumor cells killed in tumors of different shapes and sizes can be compared to determine the relative performance of thermoseed arrays to heat different tumors. Last, because there is a scalar weighting factor (γ) in the objective function that has treatment implications. the oncologist becomes an active participant in treatment planning. Reasonable estimates for the value of γ are provided. It is shown that under the assumptions of the model and based on the desired therapeutic goal. the objective function identifies a combination of seed temperatures and locations that maximizes the fraction of tumor cells killed.

REFERENCES

1. Abramowitz. M. B.; Stegun. I. A., eds. Handbook of mathematical functions with formulas, graphs, and mathematical tables. New York: Dover: 1964:358–433.

2. Arcangeli. G.; Arcangeli. G. C.; Guerra. A.; Marino, C.; Mauro. F. Tumor response to heat and radiation: Prognostic variables in the treatment of neck node metastases from head and neck cancer. Int. J. Hyperther. 1:207–217; 1985.

3. Arcangeli. G.; Lombardini. P. P.; Lovisolo. G. A.; Marsiglia. G.; Piattelli. M. Focusing of 915 MHz electromagnetic power on deep human tissues: A mathematical model study. IEEE Trans. Biomed. Eng. 31:47–52: 1984.

4. Bauer, K. D.; Henle. K. J. Arrhenius analysis of heat survival curves from normal and thermotolerant CHO cells. Radiat. Res. 78:251–263; 1979.

5. Chen. Z. P.; Roemer, R. B.; Cetas. T. C. Errors in the two-dimensional simulation of ferromagnetic implant hyperthermia. Int. J. Hyperther. 7:735–739; 1991.

6. Chin. R. B.; Stauffer. P. R. Treatment planning for ferromagnetic seed heating. Int. J. Radiat. Oncol. Biol. Phys. 21: 431–439; 1991.

7. Clegg. S. T.; Rosner, G.; Dewhirst. M. W. Hyperthermia-induced temperature distributions: A sensitivity study of cell survival (abstr.). American Sociey of Mechanical Engineers-Winter Annual Meeting, New Orleans. LA: 1993.

8. DeWagter C. Optimization of simulated two-dimensional temperature distributions induced by multiple electromagnetic applicators. IEEE Trans. Micro. Theory Tech. 34:589–596; 1986.

9. Dewey, W. C.; Hopwood. L. E.; Sapareto. S. A.; Gerweck. L. E. Cellular responses to combinations of hyperthermia and radiation. Radiology 123:463–474: 1977.

10. Dewhirst. M. W.; Sim. D. A. The utility of thermal dose as a predictor of tumor and normal tissue responses to combined radiation and hyperthermia. Cancer Res. 44 (Suppl.): 4772s–4780s: 1984.

11. Dewhirst. M. W.; Sim. D. A.; Sapareto. S.; Connor. W. G. Importance of minimum tumor temperature in determining early and long-term responses of spontaneous canine and feline tumors to heat and radiation. Cancer Res. 44:43–50: 1984.

12. Dewhirst. M. W.; Winget. J. M.; Edelstein-Keshet. L.; Sylvester. J.; Engler. M.; Thrall. D. E.; Page. R. L.; Oleson. J. R. Clinical application of thermal isoeffect dose. Int. J. Hyperther. 3:307–318; 1987.

13. Falk. P. Patterns of vasculature in two pairs of related fibrosarcomas in the rat and their relation to tumor responses to single large doses of radiation. Eur. J. Cancer 14:237–250: 1978.

14. Haider. S. A.; Cetas. T. C.; Wait. J. R.; Chen. J.-S. Power absorption in ferromagnetic implants from radio frequency magnetic fields and the problem of optimization. IEEE Trans. Micro. Theory Tech. 39:1817–1827; 1991.

15. Hall. E. J. Radiobiology for the radiologist. 3rd ed.; Philadelphia. PA: J. B. Lippincott: 1988:293–329.

16. Kapp. D. S.; Petersen. I. A.; Cox. R. S.; Hahn. G. M.; Fessenden. P.; Prionas. S. D.; Lee. E. R.; Meyer. J. L.; Samulski. T. V.; Bagshaw. M. A. Two or six hyperthermia treatments as an adjunct to radiation therapy yield similar tumor responses: Results of a randomized trial. Int. J. Radiat. Oncol. Biol. Phys. 19:1481–1495; 1990.

17. Klein. S. A.; Beckman. W. A.; Myers. G. E. FEHT: Finite element heat transfer computer program. Middleton. WI: F-chart Software: 1988–94.

18. Leopold. K. A.; Dewhirst. M.; Samulski. T.; Harrelson. J.; Tucker. J. A.; George. S. L.; Dodge. R. K.; Grant. W.; Clegg. S.; Prosnitz. L. R.; Oleson. J. R. Relationships among tumor temperature. treatment time. and histopathological outcome using preoperative hyperthermia with radiation in soft tissue sarcomas. Int. J. Radiat. Oncol. Biol. Phys. 22:989–998: 1992.

19. Mackey. M. A.; Dewey. W. C. Time-temperature analyses of cell killing of synchronous G1 and S phase Chinese hamster cells in vitro. Radiat. Res. 113:318–333: 1988.

20. Mivechi. N. F. Heat sensitivity. thermotolerance. and profile of heat shock protein synthesis of human myelogeneous leukemias. Cancer Res. 49:1954–1958: 1989.

21. Myers. G. E. Analytical methods in conduction heat transfer. Schenectady. NY: Genium Publishing Co.; 1987.

22. Nielsen. O. S.; Henle. K. J.; Overgaard. J. Arrhenius analysis of survival curves from thermotolerant and step-down heated L1A2 cells in vitro. Radiat. Res. 91:468–482: 1982.

23. Ocheltree. K. B.; Frizzell. L. A. Determination of power deposition patterns for localized hyperthermia: A transient analysis. Int. J. Hyperther. 4:281–296; 1988.

24. Oleson. J. R.; Dewhirst. M. W.; Harrelson, J. M.; Leopold. K. A.; Samulski. T. V.; Tso, C. Y. Tumor temperature distributions predict hyperthermia effect. Int. J. Radiat. Oncol. Biol. Phys. 16:559–570: 1989.

25. Oleson. J. R.; Sim. D. A.; Manning, M. R. Analysis of prognostic variables in hyperthermia treatment of 161 patients. Int. J. Radiat. Oncol. Biol. Phys. 10:2231–2239; 1984.

26. Pennes. H. H. Analysis of tissue and arterial blood temperatures in the resting human forearm. J. Appl. Physiol. 1: 93–122: 1948.

27. Robins. H. I.; Steeves. R. A.; Clark. A. W.; Martin. P. A.; Miller. K.; Dennis. W. H. Differential sensitivity of AKR murine leukemia and normal bone marrow cells to hyperthermia. Can. Res. 43:4951–4955: 1983.

28. Roemer. R. B. Heat transfer in hyperthermia treatments: Basic principles and applications. In: Paliwal. B. R.; Hetzel. F. W.; Dewhirst. M. W., eds. Biological, physical and clinical aspects of hyperthermia. New York: American Institute of Physics: 1988:210–242.

29. Rofstad. E. K.; Midthjell. H.; Brustad. T. Heat sensitivity and thermotolerance in cells from five human melanoma xenografts. Cancer Res. 44:4347–4354; 1984.

30. Steeves. R. A.; Partington. B.; Paliwal. B. R.; Brezovich. I. A. Minimum length of ferromagnetic seeds combined with ^{125}Iodine for simultaneous interstitial hyperthermia and irradiation. Abstr.: 9th Annual Meeting of the North American Hyperthermia Group: 1989:48.

31. Strohbehn. J. W.; Curtis. E. H.; Paulsen. K. D.; Yuan. X.; Lynch. D. R. Optimization of the absorbed power distribution for an annular phased array hyperthermia system. Int. J. Radiat. Oncol. Biol. Phys. 16:589–599: 1989.

32. Tompkins. D. T. A finite element heat transfer model of ferromagnetic thermoseeds and a physiologically-based objective function for pretreatment planning of ferromagnetic hyperthermia. Ph.D. Thesis: Dept. of Mechanical Engineering: University of Wisconsin–Madison: Madison. WI: 1992.

33. Tompkins. D. T.; Partington. B. P.; Steeves. R. A.; Bartholow. S. D.; Paliwal. B. R. Effect of implant variables on temperatures achieved during ferromagnetic hyperthermia. Int. J. Hyperther. 8:241–251: 1992.

34. Tompkins. D. T.; Vanderby. R.; Klein. S. A.; Beckman. W. A.; Steeves. R. A.; Paliwal. B. R. Effect of interseed spacing. tissue perfusion. thermoseed temperatures and catheters in ferromagnetic hyperthermia: Results from simulations

using finite element models of thermoseeds and catheters. IEEE Trans. Biomed. Engr. (in press).

35. van der Zee, J.; van Putten, W. L .J.; van den Berg, A. P.; van Rhoon, G. C.; Wike-Hooley, J. L.; Broekmeyer-Reurink, M. P.; Reinhold. H. S. Retrospective analysis of the response of tumors in patients treated with a combination of radiotherapy and hyperthermia. Int. J. Hyperther. 2:337–349; 1986.

36. Win-Li, L. Scan parameter optimization and a temperature controller for scanned focussed ultrasound hyperthermia:

A theoretical and experimental study. Ph.D. Thesis: Dept. of Aerospace and Mechanical Engineering; University of Arizona, Tucson. AZ; 1990.

37. Wolfram, S. Mathematica: A system for doing mathematics by computer. Champaign, IL: Wolfram Research, Inc.; 1988–94.

38. Yuan, X.; Strohbehn, J. W.; Lynch, D. R.; Johnsen, M. Theoretical investigation of a phased-array hyperthermia system with movable aperatures. Int. J. Hyperther. 6:227–240; 1990.

APPENDIX

By dividing by V_t in Eq. 6, ψ_t can be used to compare the fraction of cells killed in tumors with different volumes. As an example, consider two, one-dimensional tissue models. Tissue model 1 has a tumor length of L_{t_1} and a normal tissue length of L_{n_1}. Similarly, tissue model 2 has a tumor length of L_{t_2} ($> L_{t_1}$) and a normal tissue

length of L_{n_2} ($< L_{n_1}$). Both tissue models have a total length of L. Zero blood perfusion is assumed in the tissues for model simplicity. The thermal conductivities of the tumor and normal tissues are k_t and k_n ($> k_t$), respectively. The maximum tumor temperatures in tissue models 1 and 2 are $T_{t_1,\max}$ and $T_{t_2,\max}$, respectively. Let η_1 and η_2 denote
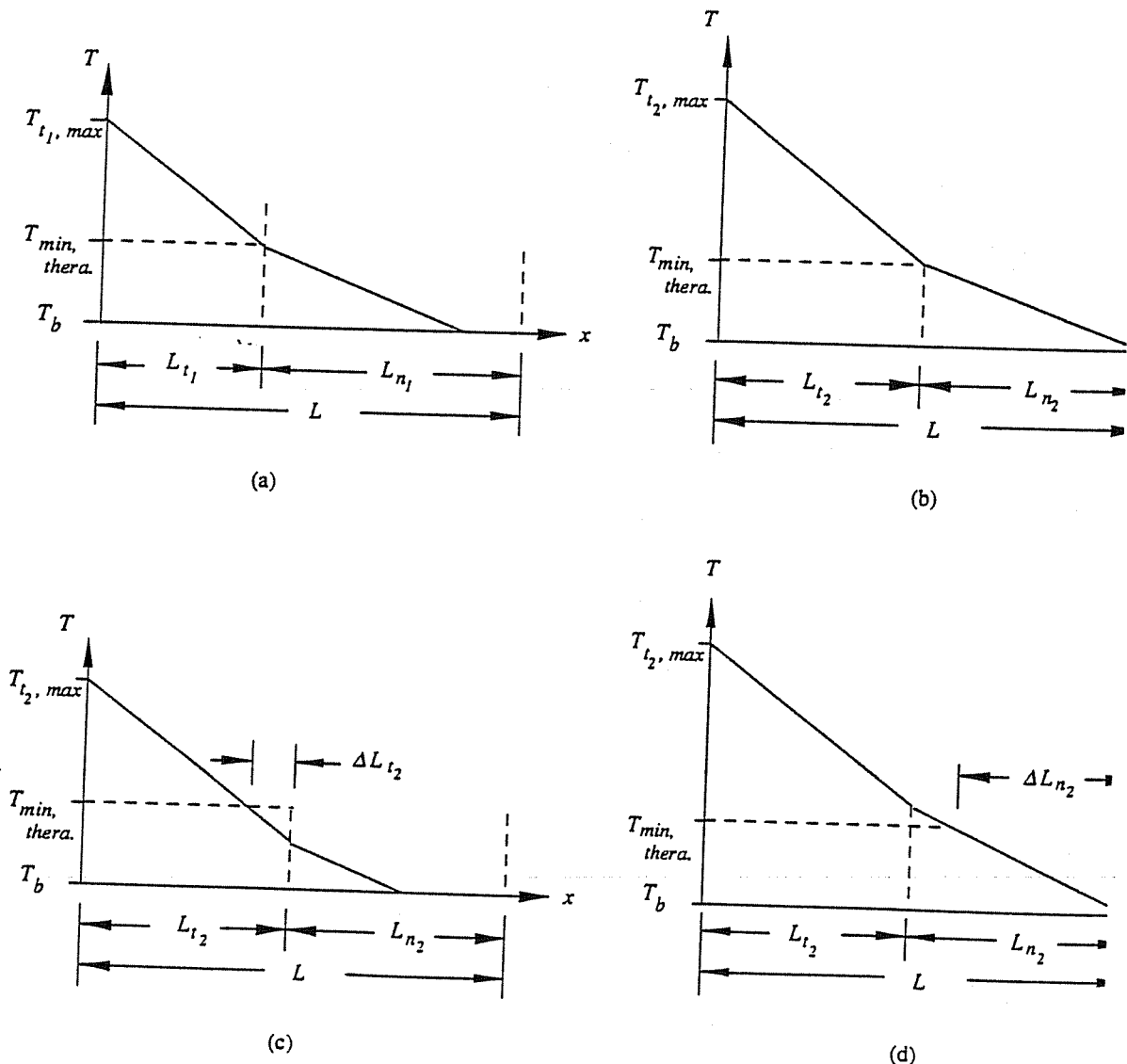

(a)

(b)

(c)

(d)

Fig. 9. Temperature profiles in one-dimensional tissue models. Tumor lengths in tissue models 1 and 2 are L_{t_1} and L_{t_2} ($> L_{t_1}$). The total length of both tissue models is L. There is no blood perfusion in these tissue models. In these figures, $T_{t_1,\max}$ (a) $= T_{t_2,\max}$ (b) $< T_{t_2,\max}$ (c and d).

the fraction of tumor cells killed in tumors 1 and 2, respectively. Three separate cases are considered:

Case 1. Consider the temperature profiles in the two tissue models shown in Fig. 9a and b. If $T_{t_1,\max} = T_{t_2,\max}$, then $\eta_1 > \eta_2$ since $L_{t_2} > L_{t_1}$. The fractions of tumor cells killed in L_{t_1} and L_{t_2} are

$$\psi_{t_1} = \frac{\eta_1 L_{t_1}}{L_{t_1}} = \eta_1$$

$$\psi_{t_2} = \frac{\eta_2 (L_{t_2} - \Delta L_{t_2})}{L_{t_2}} = \eta_2 \left(1 - \frac{\Delta L_{t_2}}{L_{t_2}} \right)$$

Because $\psi_{t_1} > \psi_{t_2}$, the temperature distribution in tumor 1 is more desirable.

Case 2. Consider the temperature profiles in the two tissue models shown in Fig. 9a and c. If $T_{t_1,\max} < T_{t_2,\max}$ so that $T_{t_1}(x = L_{t_1}) = T_{t_2}(x = L_{t_2}) = T_{\min.\text{thera}}$, then $\eta_1 < \eta_2$. Under these conditions, the fractions of tumor cells killed in L_{t_1} and L_{t_2} are

$$\psi_{t_1} = \frac{\eta_1 L_{t_1}}{L_{t_1}} = \eta_1$$

$$\psi_{t_2} = \frac{\eta_2 L_{t_2}}{L_{t_2}} = \eta_2$$

Because $\psi_{t_1} < \psi_{t_2}$, the temperature distribution in tumor 2 is more desirable.

Case 3. Consider the temperature profiles in the two tissue models shown in Fig. 9a and d. If $T_{t_1,\max} < T_{t_2,\max}$ so that $T_{t_1}(x = L_{t_1}) = T_{\min.\text{thera}} < T_{t_2}(x = L_{t_2})$, then $\eta_1 < \eta_2$. Under these conditions, the fractions of tumor cells killed in L_{t_1} and L_{t_2} are:

$$\psi_{t_1} = \frac{\eta_1 L_{t_1}}{L_{t_1}} = \eta_1$$

$$\psi_{t_2} = \frac{\eta_2 L_{t_2}}{L_{t_2}} = \eta_2$$

Because $\psi_{t_1} < \psi_{t_2}$, the temperature distribution in tumor 2 is more desirable. However, because a fraction of normal tissue cells is heated above $T_{\min.\text{thera}}$, the temperature distribution in the entire tissue system of model 2 may be less desirable than that in tissue model 1.

The arguments presented here for the one-dimensional tissue model can be extended to two- and three-dimensional models without losing the context of the conclusions in each of three cases considered.